Rare Met. (2020) 39(8):865–873
https://doi.org/10.1007/s12598-020-01452-y

RARE METALS
www.editorialmanager.com/rmet

NaV_3O_8/poly(3,4-ethylenedioxythiophene) composites as high-rate and long-lifespan cathode materials for reversible sodium storage

Guo-Chun Ding, Li-Min Zhu*, Qi Yang, Ling-Ling Xie, Xiao-Yu Cao*, Yu-Ling Wang, Jian-Ping Liu, Xin-Li Yang

Received: 16 March 2020 / Revised: 17 April 2020 / Accepted: 9 May 2020 / Published online: 18 June 2020

Abstract Sodium-ion batteries have received a surge of interests for the alternatives to lithium-ion batteries due to their abundant reserves and low cost. The quest of reliable and high-performance cathode materials is crucial to future Na storage technologies. Herein, poly(3,4-ethylenedioxythiophene) (PEDOT) was successfully introduced to NaV_3O_8 via in situ oxidation polymerization, which can effectively enhance electron conductivity and ionic diffusion of NaV_3O_8 material. As a result, these NaV_3O_8@PEDOT composites exhibit a significantly improved electrochemical performance including cycle stability and rate performance. In particular, NaV_3O_8@20 wt% PEDOT composite demonstrates better dispersibility and lower charge transfer resistance compared with bare NaV_3O_8, which delivers the first discharge capacity of 142 mAh·g^{-1} and holds about 128.7 mAh·g^{-1} after 300 cycles at a current density of 120 mA·g^{-1}. Even at a high current density of 300 mA·g^{-1}, a high reversible capacity of 99.6 mAh·g^{-1} is revealed. All these consequences suggest that NaV_3O_8@20 wt% PEDOT composite may be a promising candidate to serve as a high-rate and long-lifespan cathode material for sodium-ion batteries.

Keywords Sodium-ion batteries; NaV_3O_8@PEDOT cathode composites; In situ oxidation polymerization; High-rate; Long-lifespan

1 Introduction

Lithium resources are one of the serious restrictions for the expanding and growing future energy storage market due to their cost and reserves in earth [1–6]. Thus, it is vital to develop a novel energy storage system with sustainable development and environmental friendliness. In this regard, sodium-ion batteries (SIBs) have been extensively studied due to the natural abundance of sodium resources and the similar chemical properties of Na^+ to Li^+ [7–11]. The research investigations of anode materials for SIBs focus on carbon materials [12–15], metal [16, 17], metal oxides and metal sulfides [18–20]. A wide range of the cathode materials such as sodium metal oxides [21–23], polyanionic compounds [24–27] and organic compound [28–33], vanadium oxide and their derivatives have gained a lot of attention on account of their diversified structure and high specific capacity [34–37].

LiV_3O_8 (LVO) as a representative is widely studied in lithium-ion batteries (LIBs) and exhibits excellent electrochemical properties [38–42]. Though the radius of Na^+ is larger than that of Li^+, LVO is not suitable as cathode material for SIBs. Along this line, NaV_3O_8 (NVO) would

G.-C. Ding, L.-M. Zhu*, Q. Yang, X.-Y. Cao*, J.-P. Liu, X.-L. Yang
School of Chemistry and Chemical Engineering, Key Laboratory of High Specific Energy Materials for Electrochemical Power Sources of Zhengzhou City, Henan University of Technology, Zhengzhou 450001, China
e-mail: lmzhu@haut.edu.cn

X.-Y. Cao
e-mail: caoxy@haut.edu.cn

L.-L. Xie
School of Environmental Engineering, Key Laboratory of High Specific Energy Materials for Electrochemical Power Sources of Zhengzhou City, Henan University of Technology, Zhengzhou 450001, China

Y.-L. Wang
Department of Molecular Sciences, Australian Research Council Centre of Excellence for Nanoscale BioPhotonics, Faculty of Science and Engineering, Macquarie University, Sydney, NSW 2109, Australia

be a right choice for SIBs because of its larger interlayer distance, which is advantageous to the inserting and removing of Na^+ [43–45]. Nevertheless, NVO may be subjected to poor rate performance and cycle performance due to the slow dynamics characteristics of Na^+ and the dissolution of vanadium in the electrolyte. To improve the sluggish kinetics of the NVO for SIBs, there are many approaches which have been proposed, such as the rational design of NVO nanostructure. For example, our group reported that NVO nanorods displayed high discharge capacity of 110.4 $mAh{\cdot}g^{-1}$ at 120 $mA{\cdot}g^{-1}$, and upheld at 162.1 $mAh{\cdot}g^{-1}$ in the 500th cycle in SIBs [46]. Hu et al. [47] have synthesized NVO nanobelts and shown an outstanding electrochemical performance in LIBs, SIBs and zinc ion batteries (ZIBs). In addition, there are NVO nanowire [43], plate-type NVO [44, 48], NVO nanoflakes [45], and NVO nanobelts [49] which have been reported with superior Na storage performance. Another way is to composite with organic polymers. Kang et al. [50] successfully prepared NVO@PPy composite with core–shell structure via in situ chemical oxidation polymerization. The discharge capacity of NVO@PPy electrode maintains at 99 $mAh{\cdot}g^{-1}$ in the 60th cycle at a current density of 80 $mA{\cdot}g^{-1}$, which is considerably advanced than that of pure NVO electrode (52 $mAh{\cdot}g^{-1}$), showing excellent electrochemical performance. Relatively speaking, compositing with conduct polymer is an available and simple method to stabilize the structure of NVO by preventing vanadium dissolution and enhancing the electronic conductivity of NVO. Even more important, these composited polymers partake in electrochemical reactions and provide a certain effective capacity to some extent. All of these features are beneficial to the cyclic stability and rate performance of NVO used as electrode materials.

Poly(3,4-ethylenedioxythiophene) (PEDOT), as a common and easily synthesized electroactive polymer, has attracted wide attention and research [51–54]. However, to the best of our knowledge, the synthesis and application of NVO@PEDOT composites as cathode materials for SIBs have rarely been reported. Therefore, in this work, NVO@PEDOT composites were prepared via in situ oxidation polymerization and their electrochemical properties were systematically studied in SIBs.

2 Experimental

The pure NVO was prepared by rheological phase method [55]. Reactant $NaNO_3$, NH_4VO_3 and $C_6H_8O_7{\cdot}6H_2O$ were milled at a stoichiometric ratio of 1:3:2. Then, the powder was mixed evenly and transferred into a polytetrafluoroethylene (PTFE) container, added several drops of distilled water drop by drop under continuous stirring. Once the viscous solid–liquid rheological state occurred, the PTFE container was transferred to a stainless steel autoclave and heated for 10 h at 80 °C. Later cooling to room temperature, the PTFE container was dried again for 12 h at 100 °C. The fluffy dark green solid was obtained, scraped out for ball milling, and calcined in a 350 °C muffle furnace for 10 h. The brown–red NVO material can be obtained.

The PEDOT were prepared by oxidation polymerization. Half of aqueous $FeCl_3$ (4:1, $FeCl_3$: EDOT in mole ratio) was added into $CHCl_3$ solution and further ultrasonically treated in N_2 environment. Then, EDOT dissolved in $CHCl_3$ solution, and the mixture was added to the above solution drop by drop. After 30 min, the remaining half of $FeCl_3$ was added, and stirred for 48 h at room temperature. The reaction solution was filtered and washed repeatedly with ethanol and distilled water several times. Finally, the obtained filter cake was put in a vacuum at 80 °C for 12 h to get the target product.

NVO@PEDOT composites were synthetized via in situ oxidation polymerization. Half of aqueous $FeCl_3$ (4:1, $FeCl_3$: EDOT in mole ratio) and NVO powders were put in reaction bottle, $CHCl_3$ solution was added with ultrasonic treatment. After 10 min magnetic stirring in N_2 environment, a certain amount of EDOT (the different mass ratios of NVO to EDOT are 9:1, 8:2 and 7:3) dissolved in $CHCl_3$ solution, and this mixture was added to the above solution drop by drop. The remaining half of $FeCl_3$ was added after 30 min magnetic stirring. Then, after 48 h stirring at room temperature, the above-mentioned reaction solution was washed repeatedly with ethanol and distilled water several times. Finally, the obtained filter cake was put in a vacuum at 80 °C for 12 h to obtain dark green solid powder. For convenience, these above different proportions of NVO@PEDOT composites are recorded as NVO@10 wt% PEDOT, NVO@20 wt% PEDOT and NVO@30 wt% PEDOT, respectively.

Thermogravimetric analysis (TGA, LINSEIS SPT 1600) was used to analyze the pristine NVO, PEDOT and NVO@PEDOT composites in air from room temperature to 800 °C, and the heating rate was 10 $°C{\cdot}min^{-1}$. Structure and morphology of prepared NVO, PEDOT and NVO@-PEDOT composites were tested via powder X-ray diffraction (XRD, Rigaku MiniFlex 600), Fourier transform infrared spectroscopy (FTIR, PerkinElmer), scanning electron microscopy (SEM, FEI Quanta 250 FEG) and transmission electron microscopy (TEM, HITACHI–HT7700).

NVO or NVO@PEDOT powder, Ketjen Black and poly(vinylidene fluoride) (8:1:1 in weight ratio) were mixed in N-methyl pyrrolidone to obtain a slurry. After that, the slurry was homogeneously coated on Al foil. The CR2016-type cells were assembled in a glove box filled

with Ar. Metallic Na sheet was served as counter electrode and reference electrode, one piece of commercialized polyethylene was served as the separator and 1 mol·L^{-1} $NaClO_4$ dissolved in propylene carbonate and fluoroethylene carbonate (95:5 in volume ratio) was applied as the electrolyte. The charge–discharge tests were carried on LANHE battery tester (CT2001A) with a voltage window of 1.5–4.0 V versus Na^+/Na. Cyclic voltammetry (CV) and electrochemical impedance spectroscopy (EIS) were tested on electrochemical workstation (CHI 660D). The capacities and current densities were calculated based on the NVO@PEDOT composite mass loading.

3 Results and discussion

3.1 Structure and composition characterization

The content of PEDOT in NVO@PEDOT composites was analyzed and calculated by TGA test. As presented in Fig. 1a, the mass loss of NVO is about 5% at 100 °C, which may be caused by the removal of adsorbed water in the material. PEDOT began to decompose at 200 °C and decompose completely until 500 °C with a mass loss of about 71.8%. Compared with NVO material, the mass loss in NVO@PEDOT composites can be attributed to the decomposition of PEDOT at high temperature [40]. Therefore, according to the actual total mass of NVO and experimental data, the actual content of PEDOT in NVO@10 wt% PEDOT, NVO@20 wt% PEDOT and NVO@30 wt% PEDOT were calculated to be 12.4 wt%, 22.4 wt% and 30.5 wt%, respectively, which shows that the composited NVO@PEDOT composites meet our expectations.

The composite structure of NVO@PEDOT was further verified by FTIR (Fig. 1b). For pure PEDOT, the characteristic peaks at about 1511 and 1342 cm^{-1} are the skeleton vibrations of thiophene ring and the stretching vibration of C–C and C=C, and characteristic absorption peaks of C–O–C on polymer chain skeleton appear at 1192 and 1062 cm^{-1}. Moreover, three characteristic absorption peaks at 980, 840 and 688 cm^{-1} correspond to the C-S bond vibration on the thiophene ring [56–58]. In the FTIR spectra of NVO, there are two peaks at 991 and 953 cm^{-1}, belonging to the stretching vibration of V=O bond, while characteristic peaks appear at 747 and 570 cm^{-1}, attributing to the symmetrical stretching vibration of V–O–V bond and the asymmetrical stretching vibration of V–O–V bond, respectively [59, 60]. The spectra of NVO@20 wt% PEDOT composite displays that there are not only characteristic peaks of NVO, but also that of PEDOT, we can conclude that NVO@20 wt% PEDOT composite has been successfully synthesized.

XRD diagram of NVO and NVO@PEDOT composites with different compositing ratios are presented in Fig. 2. The diffraction peaks of NVO and NVO@PEDOT composites correspond to the standard card (JCPDS No. 35-0436) besides a weak superfluous peak at $2\theta = 12.02°$, which can be belonged to NaV_6O_{15} (JCPDS No. 28-1172) [61]. In addition, we have not found the diffraction peak of PEDOT in the composites, which states clearly that PEDOT exists in amorphous state and PEDOT does not affect the original structure of NVO.

3.2 Morphology characterization

The morphologies of NVO and NVO@PEDOT composites were studied by a combination of SEM and TEM test. PEDOT sample manifests irregular aggregation block and the surface size is about 1 μm; however, the NVO powder displays a rod structure with a length of ~ 1 μm. Compared with bare NVO, NVO@PEDOT shows that interlaced particles are connected by PEDOT network structure (Fig. 3a–e), but the particle size of NVO@PEDOT

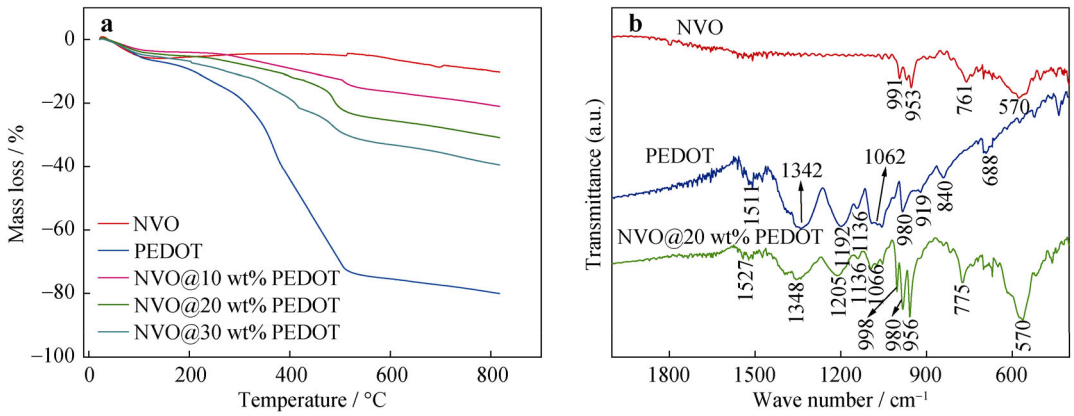

Fig. 1 **a** TGA curves of NVO, PEDOT and NVO@PEDOT composites; **b** FTIR spectra of NVO, PEDOT and NVO@20 wt% PEDOT composite

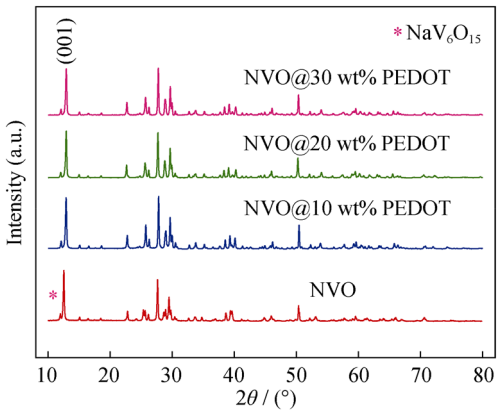

Fig. 2 XRD patterns of NVO and NVO@PEDOT composites

increases gradually. Agglomeration occurred and NVO micro-nanorods were disappeared with the increase in the composited content of PEDOT, which was adverse to the electrochemical reaction of NVO in the charging and discharging process. Through the above comparison, we tentatively put forward that suitable quantity of PEDOT will play a significant role. Among them, it is confirmed that NVO@20 wt% PEDOT material shows better dispersibility and no large reunion. In addition, it can be discovered from TEM images in Fig. 3f, g, PEDOT evenly coated on NVO rod and some filled in the NVO rod gap, thus effectively increasing the links between NVO rod. All these findings will be propitious to increase the transport rate of Na^+ and electronics in NVO material, which will favor the electrochemical performance of NVO. Energy-dispersive X-ray spectroscopy (EDS) mapping results in Fig. 3h depicted the existence of C, O and S, which proved that PEDOT is successfully composited with NVO as well.

3.3 Electrochemical performances

The initial discharge profiles of NVO and NVO@PEDOT composites were evaluated between 1.5 and 4.0 V at a current density of 120 $mA \cdot g^{-1}$ (Fig. 4a). It is clearly seen that the discharge platforms of composites rise first and then decrease with the increase in the mass loading of PEDOT. Moreover, compared with NVO, the composites have more platforms because PEDOT may be also involved in the reaction. The first discharge capacities of

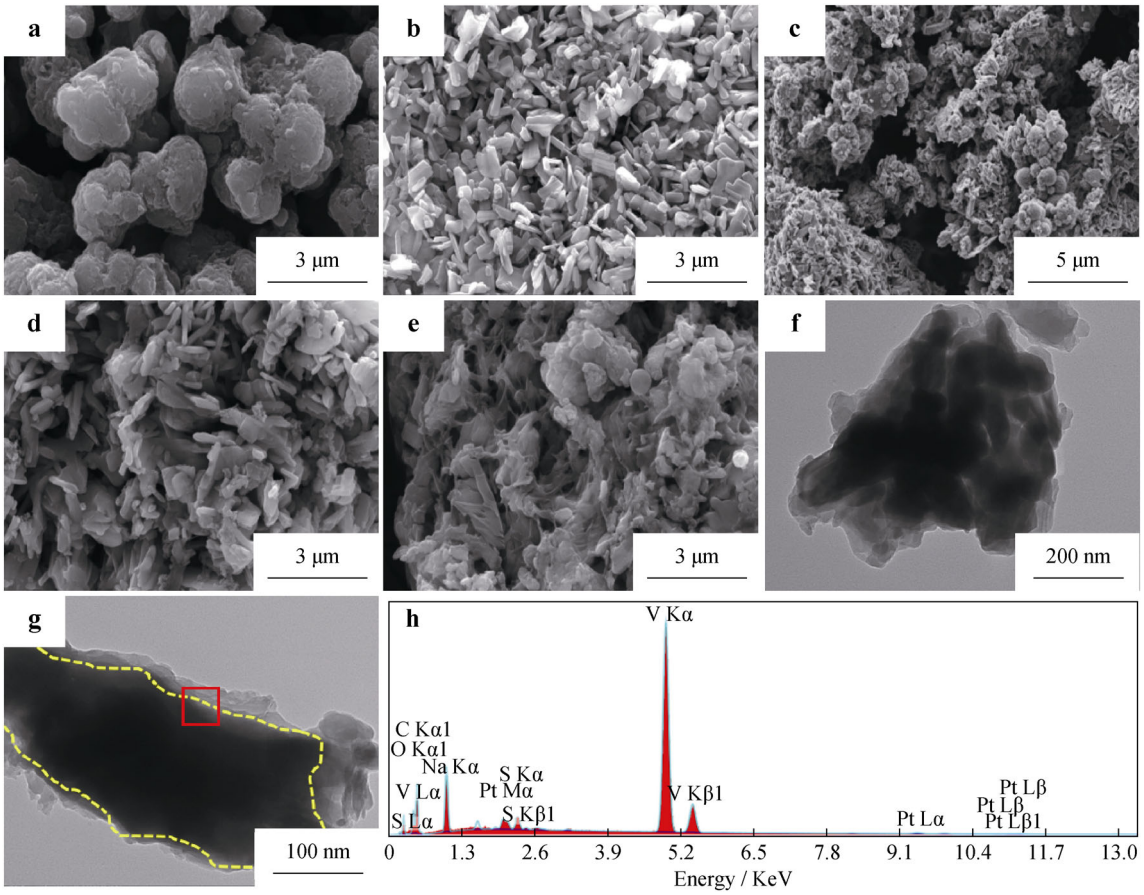

Fig. 3 SEM images of **a** PEDOT, **b** NVO, **c** NVO@10 wt% PEDOT composite, **d** NVO@20 wt% PEDOT composite and **e** NVO@30 wt% PEDOT composite; **f, g** TEM images of NVO@20 wt% PEDOT composite; **h** EDS results of NVO@20 wt% PEDOT composite

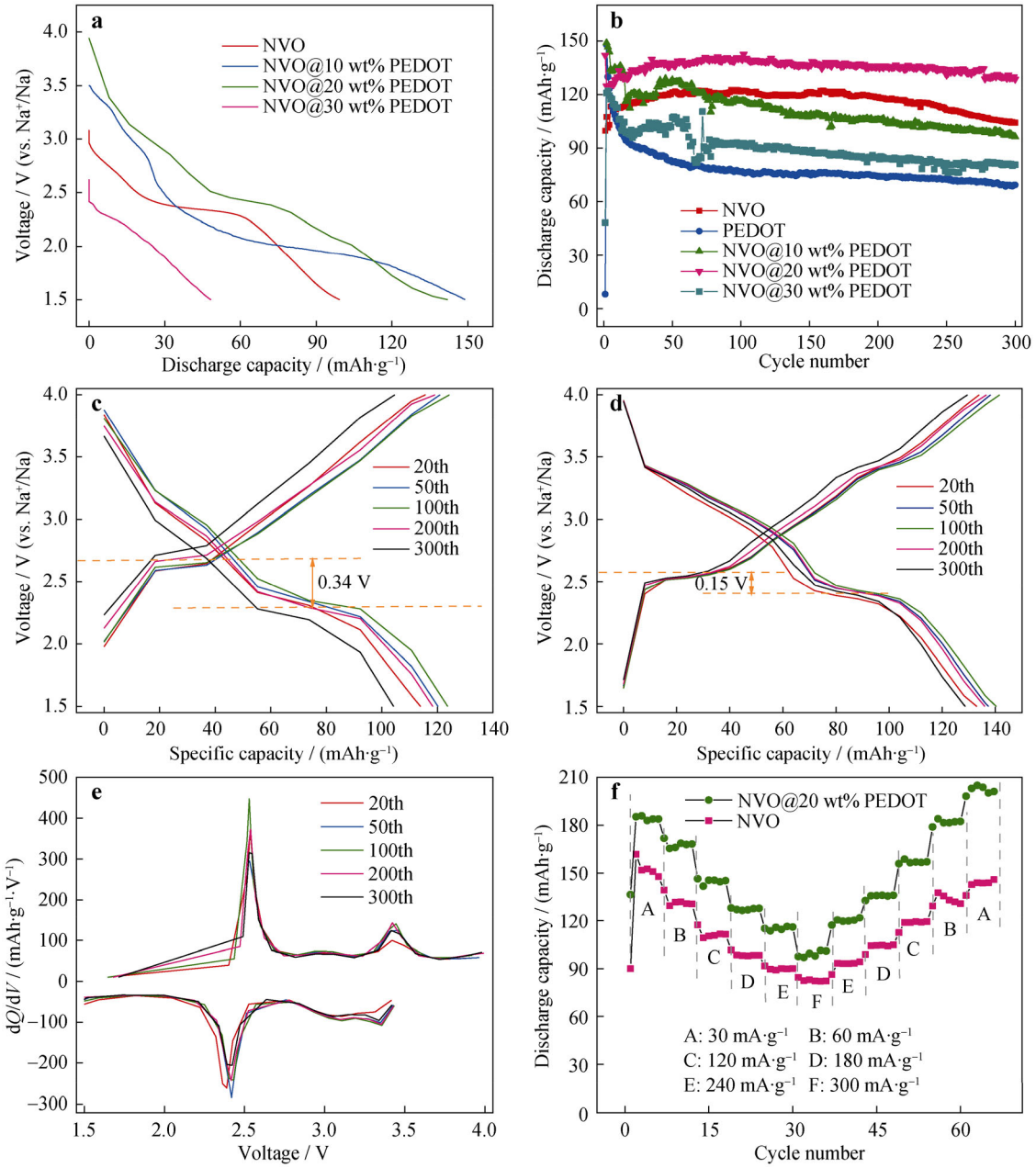

Fig. 4 **a** Initial discharge curves of NVO and NVO@PEDOT composites; **b** cycle performances of NVO and NVO@PEDOT composites; charge–discharge curves at different cycles the voltage range of 1.5–4.0 V at 120 mA·g^{-1}: **c** NVO and **d** NVO@20 wt% PEDOT composite; **e** differential capacity curves of NVO@20 wt% PEDOT composite at same conditions; **f** rate capabilities of NVO and NVO@20 wt% PEDOT composite at various current densities

NVO, NVO@10 wt% PEDOT, NVO@20 wt% PEDOT and NVO@30 wt% PEDOT are 99.2, 148.9, 142 and 48.3 mAh·g^{-1}, respectively. Although the initial capacity of NVO@10 wt% PEDOT is higher than that of NVO@20 wt% PEDOT, the plateau potential of NVO@20 wt% PEDOT is higher, and it is observed from Fig. 4b that the capacity of NVO@20 wt% PEDOT is the highest after 300 cycles, which is maintained at 128.7 mAh·g^{-1}. However, NVO, NVO@10 wt% PEDOT and NVO@30 wt% PEDOT maintained at 104.2, 96.3 and 80.6 mAh·g^{-1}, respectively. These results indicate that appropriate PEDOT compositing supported in outstanding structural stability and attaining higher and reversible capacity.

Figure 4c, d exhibit the charge–discharge curves of NVO and NVO@20 wt% PEDOT at the selected cycles. NVO and NVO@20 wt% PEDOT composite in the 20th, 50th, 100th, 200th and 300th cycles deliver capacities of 115.6, 121.2, 121.6, 118.6, 104.2 mAh·g^{-1} and 133.0,

137.4, 140.3, 136.0 and 128.7 mAh·g^{-1}, respectively. Besides, compared with one of the charging and discharging platforms, the potential difference of NVO@20 wt% PEDOT is much lower than that of NVO. From this point of view, it is proved again that PEDOT can effectively stabilize the structure of NVO, increase capacity and reduce the electrochemical polarization. In addition, the differential capacity curves of NVO@20 wt% PEDOT composite are nearly overlapped within 300 cycles (Fig. 4e), indicating extremely stable and reversible chemical reaction. These results imply that it is feasible to improve the electrochemical performance of NVO via PEDOT compositing.

Moreover, the NVO@20 wt% PEDOT composite also displays outstanding improvement rate capability, and the results are represented in Fig. 4f. The average discharge specific capacities of NVO are about 152, 131, 111, 98, 90 and 83 mAh·g^{-1} with the current densities increasing from 30 to 300 mA·g^{-1} step by step. As soon as the current density returns to 30 mA·g^{-1}, the average discharge specific capacity is ~ 143 mAh·g^{-1}, which decreased compared with the first discharge capacity, and the capacity retention is 94%. In contrast, the average discharge specific capacities of NVO@20 wt% PEDOT composite are about 184, 167, 145, 127, 114 and 98 mAh·g^{-1} at the same condition. When the current density returns to 30 mA g^{-1}, the average discharge specific capacity is ~ 202 mAh·g^{-1}, which is higher than the first discharge capacity, and the capacity retention is as high as 109.8%. These results clearly reveal that the composite has less polarization and excellent redox reversibility, which could be attributed to the suitable amount of PEDOT, and the Na^+ mobility and electronic conductivity can be effectively improved.

CV curves of NVO from the first cycle to the fourth cycle (0.3 mV·s^{-1}) demonstrate three pairs of redox peaks at about 2.59/2.27, 3.16/2.83 and 3.46/3.34 V (Fig. 5a). Although these peaks position and intensity did not change after 4 cycles, the symmetry of peak area was poor. Similarly, NVO@20 wt% PEDOT electrode also shows three pairs of main redox peaks at 2.63/2.31, 3.02/2.98 and 3.53/3.34 V (Fig. 5b), the peak area is much more symmetrical, and the potential gap of redox peaks is narrow, revealing the high reversibility of the composited electrode.

Figure 6a depicts EIS spectra of the NVO and NVO@20 wt% PEDOT electrodes at open-circuit voltage. The equivalent circuit mainly consists of electrolyte resistance (R_s), charge transfer resistance (R_{ct}), constant phase element (CPE), the impedance of electrons transfer (R_f) and Warburg impedance (W_s). As shown, all Nyquist plots display one semicircle and a low-frequency Warburg tail, corresponding to the resistance of the charge transfer (R_{ct}) and the resistance of Na^+ diffusion in the bulk materials (Z_ω) [62–64]. The R_{ct} values of NVO and NVO@20 wt% PEDOT are 472 and 188 Ω, respectively, the NVO@20 wt% PEDOT composite confirmed the lower R_{ct} compared with bare NVO. On the basis of the equation ($D_{Na^+}=0.5R^2T^2/S^2n^4F^4C^2\sigma^2$) [38], where R is the gas constant, T is Kelvin temperature (298 K), S is the surface area (1.13 cm^2), n is the numbers of electrons exchanged per molecule during oxidization, F is Faraday constant, C is the concentration of Na^+ calculated in view of the crystallographic cell parameter of NVO, σ is the slope of the line in Fig. 6b, ω is the angular frequency at low frequency, the diffusion coefficients (D_{Na^+}) of bare NVO and NVO@20 wt% PEDOT composite at open-circuit voltage are 1.17 × 10^{-14} and 2.38 × 10^{-14} cm^2·s^{-1}. These findings reveal that NVO@20 wt% PEDOT composite has smaller resistance of charge transfer and faster charge–discharge ability, proving that the NVO@20 wt% PEDOT has better electrochemistry performance as above mentioned.

According to all these analyses, the schematic illustration of transfer pathway of Na^+ and electrons in the NVO and NVO@PEDOT composites are presented in Scheme 1.

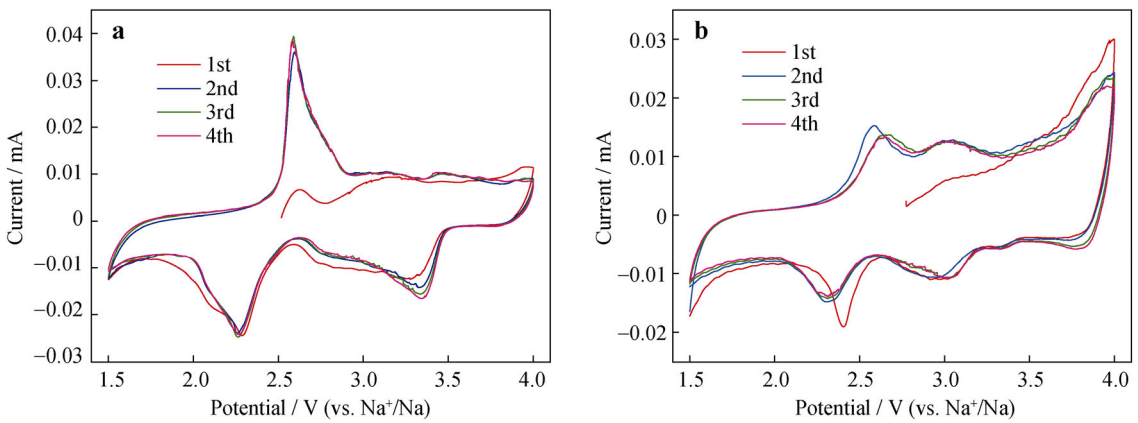

Fig. 5 First four cycles of CV at scan speed of 0.3 mV·s^{-1}: **a** NVO and **b** NVO@20 wt% PEDOT composite

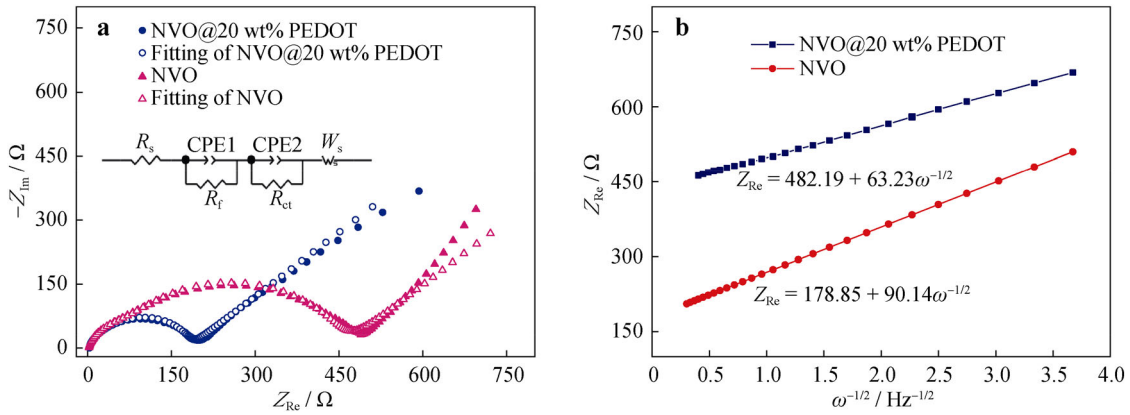

Fig. 6 **a** Nyquist plots of NVO and NVO@20 wt% PEDOT composite at open-circuit potential; **b** relationship curves between Z_{Re} and $\omega^{-1/2}$ in low-frequency range of NVO and NVO@20 wt% PEDOT composite

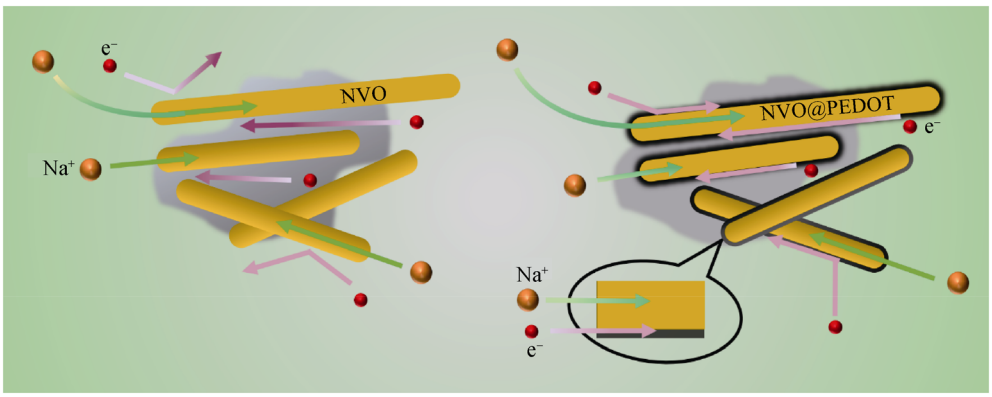

Scheme 1 Schematic illustration of transfer pathway of Na^+ and electron in NVO and NVO@PEDOT composites

PEDOT acts as an important conductive network role in the composites, ensuring the fast transfer of electrons and Na^+ ions between active substances.

In general, proper amount of PEDOT is very useful for improving the electrochemistry performance of NVO. First, appropriate PEDOT reduces resistance of charge transfer and improves the electrons conduction, thus the rate performance of NVO can be improved. Second, structural stability of NVO is ensured by PEDOT, so then the charge–discharge stability of NVO can be improved. In short, the introduction of PEDOT effectively overcomes the shortcomings of NVO, the NVO@20 wt% PEDOT composite electrode displayed a greatly improved performance such as good cycle stability, high reversible capacity and rate capacity.

4 Conclusion

In this work, NVO@ PEDOT composites have been effectively obtained through a simple in situ oxidation polymerization. It has been verified that electrochemical properties of NVO could be improved with long cycle life, high reversible and rate capacity by PEDOT modification. The prepared NVO@20 wt% PEDOT composite carries the first discharge capacity of 142 $mAh \cdot g^{-1}$ at 120 $mA \cdot g^{-1}$ between 1.5 and 4.0 V, and holds 128.7 $mAh \cdot g^{-1}$ after 300 cycles. Even at 300 $mA \cdot g^{-1}$, it continues to reveal a high reversible capacity of 99.6 $mAh \cdot g^{-1}$. The meaningfully improved performance of the NVO@20 wt% PEDOT may be attributed to the introduction of appropriate amount of PEDOT. Here, PEDOT serves as protective layer to defend NVO during charge–discharge, which results in a better cyclic stability. PEDOT also reduces the R_{ct} and improves the diffusion coefficient (D_{Na^+}), which results in high reversible capacity and decent rate performance. This work provides a simple and effective synthesis method, which can be transformative to design and prepare other vanadium-based compounds for SIBs.

Acknowledgements This study was financially supported by the National Natural Science Foundation of China (Nos. 21773057, U1704142 and U1904216), the Postdoctoral Science Foundation of China (No. 2017M621833), Zhongyuan Thousand People Plan-The Zhongyuan Youth Talent Support Program (in Science and

Technology) of China (No. ZYQR201810139), the Program for Science and Technology Innovation Talents in Universities of Henan Province, China (No. 18HASTIT008) and the Fundamental Research Funds in Henan University of Technology (No. 2018RCJH01).

References

[1] Wu D, Zhang W, Feng Y, Ma J. Necklace-like carbon nanofibers encapsulating V_3S_4 microspheres for ultrafast and stable potassium-ion storage. J Mater Chem A. 2020;8(5):2618.
[2] Song T, Yao W, Kiadkhunthod P, Zheng Y, Wu N, Zhou X, Tunmee S, Sattayaporn S, Tang Y. A low-cost and environmentally friendly mixed polyanionic cathode for sodium-ion storage. Angew Chem Int Ed. 2020;59(2):740.
[3] Lan Y, Yao W, He X, Song T, Tang Y. Mixed polyanionic compounds as positive electrodes in low-cost electrochemical energy storage. Angew Chem Int Ed. 2020. https://doi.org/10.1002/anie.201915666.
[4] Hong W, Zhang Y, Yang L, Tian Y, Ge P, Hu J, Wei W, Zou G, Hou H, Ji X. Carbon quantum dot micelles tailored hollow carbon anode for fast potassium and sodium storage. Nano Energy. 2019;65:104038.
[5] Yang J, Wan HL, Zhang ZH, Liu GZ, Xu XX, Hu YS, Yao XY. NASICON-structured $Na_{3.1}Zr_{1.95}Mg_{0.05}Si_2PO_{12}$ solid electrolyte for solid-state sodium batteries. Rare Met. 2018;37(6):480.
[6] Du M, Chen M, Yang XG, Wen J, Wang X, Fang SM, Liu CS. A channel-type mesoporous In(III)–carboxylate coordination framework with high physicochemical stability for electrode material of supercapacitor. J Mater Chem A. 2014;2(25):9828.
[7] Liu GQ, Li Y, Du YL, Wen L. Synthesis and properties of $Na_{0.8}Ni_{0.4}Mn_{0.6}O_2$ oxide used as cathode material for sodium ion batteries. Rare Met. 2017;36(12):977.
[8] Luo W, Gaumet JJ, Mai LQ. Antimony-based intermetallic compounds for lithium-ion and sodium-ion batteries: synthesis, construction and application. Rare Met. 2017;36(5):321.
[9] Cheng DL, Yang LC, Zhu M. High-performance anode materials for Na-ion batteries. Rare Met. 2018;37(3):167.
[10] Xu B, Qi S, Li F, Peng X, Cai J, Liang J, Ma J. Cotton-derived oxygen/sulfur co-doped hard carbon as advanced anode material for potassium-ion batteries. Chin Chem Lett. 2020;31(1):217.
[11] Pu X, Wang H, Zhao D, Yang H, Ai X, Cao S, Chen Z, Cao Y. Recent progress in rechargeable sodium-ion batteries: toward high-power applications. Small. 2019;15(32):1805427.
[12] Tang K, Fu L, White RJ, Yu L, Titirici MM, Antonietti M, Maier J. Hollow carbon nanospheres with superior rate capability for sodium-based batteries. Adv Energy Mater. 2017;2(7):873.
[13] Zhu Y, Li J, Yun X, Zhao G, Ge P, Zou G, Liu Y, Hou H, Ji X. Graphitic carbon quantum dots modified nickel cobalt sulfide as cathode materials for alkaline aqueous batteries. Nano-Micro Lett. 2020;12(1):16.
[14] Hou H, Banks CE, Jing M, Zhang Y, Ji X. Carbon quantum dots and their derivative 3D porous carbon frameworks for sodium-ion batteries with ultralong cycle life. Adv Mater. 2015;27(47):7861.
[15] Ge P, Hou H, Cao X, Li S, Zhao G, Guo T, Wang C, Ji X. Multidimensional evolution of carbon structures underpinned by temperature-induced intermediate of chloride for sodium-ion batteries. Adv Sci. 2018;5(6):1800080.
[16] Ge P, Li S, Shuai H, Xu W, Tian Y, Yang L, Zou G, Hou H, Ji X. Ultrafast sodium full batteries derived from X–Fe (X = Co, Ni, Mn) prussian blue analogs. Adv Mater. 2019;31(3):1806092.
[17] Wang L, Wang Z, Xie L, Zhu L, Cao X. ZIF-67-derived N-doped Co/C nanocubes as high-performance anode materials for lithium-ion batteries. ACS Appl Mater Interfaces. 2019;11(18):16619.
[18] Zhang Y, Foster CW, Banks CE, Shao L, Hou H, Zou G, Chen J, Huang Z, Ji X. Graphene-rich wrapped petal-like rutile TiO_2 tuned by carbon dots for high-performance sodium storage. Adv Mater. 2016;28(42):9391.
[19] Ge P, Zhang C, Hou H, Wu B, Zhou L, Li S, Wu T, Hu J, Mai L, Ji X. Anions induced evolution of Co_3X_4 (X = O, S, Se) as sodium-ion anodes: the influences of electronic structure, morphology, electrochemical property. Nano Energy. 2018;48:617.
[20] Ge P, Hou H, Li S, Yang L, Ji X. Tailoring rod-like $FeSe_2$ coated with nitrogen-doped carbon for high-performance sodium storage. Adv Funct Mater. 2018;28(30):1801765.
[21] Gao X, Jiang F, Yang Y, Zhang Y, Zou G, Hou H, Hu Y, Sun W, Ji X. Chalcopyrite-derived Na_xMO_2 (M = Cu, Fe, Mn) cathode: tuning impurities for self-doping. ACS Appl Mater Interfaces. 2020;12(2):2432.
[22] Yabuuchi N, Ikeuchi I, Kubota K, Komaba S. Thermal stability of Na_xCrO_2 for rechargeable sodium batteries; studies by high-temperature synchrotron X-ray diffraction. ACS Appl Mater Interfaces. 2018;8(47):32292.
[23] Ortiz-Vitoriano N, Drewett NE, Gonzalo E, Rojo T. High performance manganese-based layered oxide cathodes: overcoming the challenges of sodium ion batteries. Energy Environ Sci. 2017;10(5):1051.
[24] Fang Y, Zhang J, Xiao L, Ai X, Cao Y, Yang H. Phosphate framework electrode materials for sodium ion batteries. Adv Sci. 2017;4(5):1600392.
[25] Cao X, Sun Q, Zhu L, Xie L. $Na_3V_2(PO_4)_3$ nanoparticles confined in functional carbon framework towards high-rate and ultralong-life sodium storage. J Alloys Compd. 2019;791:296.
[26] Fang Y, Liu Q, Xiao L, Rong Y, Liu Y, Chen Z, Ai X, Cao Y, Yang H, Xie J, Sun C, Zhang X, Aoun B, Xing X, Xiao X, Ren Y. A fully sodiated $NaVOPO_4$ with layered structure for high-voltage and long-lifespan sodium-ion batteries. Chem. 2018;4(5):1167.
[27] Ni Q, Bai Y, Wu F, Wu C. Polyanion-type electrode materials for sodium-ion batteries. Adv Sci. 2017;4(3):1600275.
[28] Cao X, Liu J, Zhu L, Xie L. Polymer electrode materials for high-performance lithium/sodium-ion batteries: a review. Energy Technol. 2019;7(7):1800759.
[29] Zhu L, Shen Y, Sun M, Qian J, Cao Y, Ai X, Yang H. Self--doped polypyrrole with ionizable sodium sulfonate as a renewable cathode material for sodium ion batteries. Chem Commun. 2013;49(97):11370.
[30] Zhu L, Liu J, Liu Z, Xie L, Cao X. Anthraquinones with ionizable sodium sulfonate groups as renewable cathode materials for sodium-ion batteries. ChemElectroChem. 2019;6(3):787.
[31] Muench S, Wild A, Friebe C, Häupler B, Janoschka T, Schubert US. Polymer-based organic batteries. Chem Rev. 2016;116(16):9438.
[32] Novák P, Müller K, Santhanam K, Haas O. Electrochemically active polymers for rechargeable batteries. Chem Rev. 1997;97(1):207.
[33] Zhu L, Ding G, Liu J, Liu Z, Xie L, Cao X. Graphene-wrapped poly(2,5-dihydroxy-1,4-benzoquinone-3,6-methylene) nanoflowers as low-cost and high-performance cathode materials for sodium-ion batteries. Int J Energy Res. 2019;43(13):7635.
[34] Ko YN, Kang YC, Park SB. A new strategy for synthesizing yolk-shell V_2O_5 powders with low melting temperature for high performance Li-ion batteries. Nanoscale. 2013;5(19):8899.
[35] Yu H, Rui X, Tan H, Chen J, Huang X, Xu C, Liu W, Yu DYW, Hng HH, Hoster HE, Yan Q. Cu doped V_2O_5 flowers as cathode material for high-performance lithium ion batteries. Nanoscale. 2013;5(11):4937.

[36] Chen Z, Cao L, Chen L, Zhou H, Xie K, Kuang Y. Nanoplate-stacked baguette-like $LiVO_3$ as a high performance cathode material for lithium-ion batteries. J Mater Chem A. 2015;3(16):8750.
[37] Weckhuysen BM, Keller DE. Chemistry, spectroscopy and the role of supported vanadium oxides in heterogeneous catalysis. Catal Today. 2003;78(1):25.
[38] Zhu L, Xie L, Cao X. LiV_3O_8/polydiphenylamine composites with significantly improved electrochemical behavior as cathode materials for rechargeable lithium batteries. ACS Appl Mater Interfaces. 2018;10(13):10909.
[39] Zhu L, Li W, Xie L, Cao X. LiV_3O_8/poly(1,5-diaminoanthraquinone) composite as a high performance cathode material for rechargeable lithium batteries. Mater Lett. 2017;206:225.
[40] Zhu L, Li W, Yu Z, Xie L, Cao X. Synthesis and electrochemical performances of LiV_3O_8/poly(3,4-ethylenedioxythiophene) composites as cathode materials for rechargeable lithium batteries. Solid State Ionics. 2017;310:30.
[41] Chen Z, Xu F, Cao S, Li Z, Yang H, Ai X, Cao Y. High rate, long lifespan LiV_3O_8 nanorods as a cathode material for lithium-ion batteries. Small. 2017;13(18):1603148.
[42] Song H, Luo M, Wang A. High rate and stable li-ion insertion in oxygen-deficient LiV_3O_8 nanosheets as a cathode material for lithium-ion battery. ACS Appl Mater Interfaces. 2017;9(3):2875.
[43] Zhu L, Ding G, Xie L, Yang Q, Yang X, Cao X. Facile preparation of NaV_3O_8/polytriphenylamine composites as cathode materials towards high-performance sodium storage. Int J Energy Res. 2020;44(4):3215.
[44] Cao L, Chen L, Huang Z, Kuang Y, Zhou H, Chen Z. NaV_3O_8 nanoplates as a lithium-ion battery cathode with superior rate capability and cycle stability. ChemElectroChem. 2016;3(1):122.
[45] Tang Y, Sun D, Wang H, Huang X, Zhang H, Liu S, Liu Y. Synthesis and electrochemical properties of NaV_3O_8 nanoflakes as high-performance cathode for Li-ion battery. RSC Adv. 2014;4(16):8328.
[46] Zhu L, Li W, Xie L, Yang Q, Cao X. Rod-like NaV_3O_8 as cathode materials with high capacity and stability for sodium storage. Chem Eng J. 2019;372:1056.
[47] Hu F, Xie D, Cui F, Zhang D, Song G. Synthesis and electrochemical performance of NaV_3O_8 nanobelts for Li/Na-ion batteries and aqueous zinc-ion batteries. RSC Adv. 2019;9(36):20549.
[48] Diem N, Gim J, Mathew V, Song J, Kim S, Ahn D, Kim J. Plate-type NaV_3O_8 cathode by solid sate reaction for sodium-ion batteries. ECS Electrochem Lett. 2014;3(7):A69.
[49] Rashad M, Li X, Zhang H. Magnesium/lithium-ion hybrid battery with high reversibility by employing NaV_3O_8 center dot 1.$69H_2O$ nanobelts as a positive electrode. ACS Appl Mater Interfaces. 2018;10(25):21313.
[50] Kang H, Liu Y, Shang M, Lu T, Wang Y, Jiao L. NaV_3O_8 nanosheet@polypyrrole core-shell composites with good electrochemical performance as cathodes for Na-ion batteries. Nanoscale. 2015;7(20):9261.
[51] Meng H, Perepichka DF, Wudl F. Facile solid-state synthesis of highly conducting poly(ethylenedioxythiophene). Angew Chem Int Ed. 2003;42(6):658.
[52] Yang H, Liu Y, Wang Z, Liu Y, Du H, Hao X. A highly oriented poly(3,4-ethylenedioxythiophene) film: facile synthesis and application for supercapacitor. J Appl Polym Sci. 2016;133(20):43418.
[53] Jiang X, Yu Z, Zhang Y, Lai J, Li J, Gurzadyan GG, Yang X, Sun L. High-performance regular perovskite solar cells employing low-cost poly(ethylenedioxythiophene) as a hole-transporting material. Sci Rep. 2017;7:42564.
[54] Rumbau V, Pomposo JA, Eleta A, Rodriguez J, Grande H, Mecerreyes D, Ochoteco E. First enzymatic synthesis of water-soluble conducting poly(3,4-ethylenedioxythiophene). Biomacromolecules. 2007;8(2):315.
[55] Cao X, Yang Q, Zhu L, Xie L. NaV_3O_8 with superior rate capability and cycle stability as cathode materials for sodium-ion batteries. Ionics. 2018;24(3):943.
[56] Xu J, Nie G, Zhang S, Han X, Hou J, Pu S. Electrochemical copolymerization of indole and 3,4-ethylenedioxythiophene. J Mater Sci. 2005;40(11):2867.
[57] Fabregat G, Estrany F, Casas MT, Alemán C, Armelin E. Detection of dopamine using chemically synthesized multilayered hollow microspheres. J Phys Chem B. 2014;118(17):4702.
[58] Zhan L, Song Z, Zhang J, Tang J, Zhan H, Zhou Y, Zhan C. PEDOT: cathode active material with high specific capacity in novel electrolyte system. Electrochim Acta. 2008;53(28):8319.
[59] Yang G, Hou W, Sun Z, Yan Q. A novel inorganic–organic polymer electrolyte with a high conductivity: insertion of poly(ethylene) oxide into LiV_3O_8 in one step. J Mater Chem. 2005;15(13):1369.
[60] Koval'chuk EP, Reshetnyak OV, Kovalyshyn YS, Blażejowski J. Structure and properties of lithium trivanadate-a potential electroactive material for a positive electrode of secondary storage. J Power Sour. 2002;107(1):61.
[61] Wang H, Liu S, Ren Y, Wang W, Tang A. Ultrathin $Na_{1.08}V_3O_8$ nanosheets-a novel cathode material with superior rate capability and cycling stability for Li-ion batteries. Energy Environ Sci. 2012;5(3):6173.
[62] Li J, Wei H, Peng Y, Geng L, Zhu L, Cao X, Liu C, Pang H. A multifunctional self-healing G-PyB/KCl hydrogel: smart conductive, rapid room-temperature phase-selective gelation, and ultrasensitive detection of alpha-fetoprotein. Chem Commun. 2019;55:7922.
[63] Liu T, Zhao SX, Gou LL, Wu X, Nan CW. Electrochemical performance of Li-rich cathode material, $0.3Li_2MnO_3$–$0.7LiMn_{1/3}Ni_{1/3}Co_{1/3}O_2$ microspheres with F-doping. Rare Met. 2019;38(3):189.
[64] Zhou HM, Zhu YH, Li J, Sun WJ, Liu ZZ. Electrochemical performance of Al_2O_3 pre-coated spinel $LiMn_2O_4$. Rare Met. 2019;38(2):128.